High- and Low-Temperature Crystal and Magnetic Structures of ϵ-Fe_2O_3 and Their Correlation to Its Magnetic Properties

M. Gich,* C. Frontera, A. Roig, E. Taboada, and E. Molins

Institut de Ciència de Materials de Barcelona, Consejo Superior de Investigaciones Científicas, Campus de la UAB, 08193 Bellaterra, Catalunya, Spain

H. R. Rechenberg

Instituto de Física, Universidade de São Paulo, Caixa Postal 66318, 05315-970 São Paulo, Brazil

J. D. Ardisson and W. A. A. Macedo

Laboratório de Física Aplicada, Centro de Desenvolvimento da Tecnologia Nuclear, 31270-901 Belo Horizonte, Brazil

C. Ritter

Institut Laue-Langevin, 6 rue Jules Horowitz, BP 156, 38042 Grenoble Cedex, France

V. Hardy

Laboratoire CRISMAT/ENSICAEN, UMR 6508 du CNRS, 6 Bd Marechal Juin, 14050 Caen, France

J. Sort, V. Skumryev, and J. Nogués

Institució Catalana de Recerca i Estudis Avançats (ICREA) and Departament de Física, Universitat Autònoma de Barcelona, 08193 Bellaterra, Catalunya, Spain

Received April 28, 2006. Revised Manuscript Received June 1, 2006

The crystal and magnetic structures of orthorhombic ϵ-Fe_2O_3 have been studied by simultaneous Rietveld refinement of X-ray and neutron powder-diffraction data in combination with Mössbauer spectroscopy, as well as magnetization and heat-capacity measurements. It has been found that above 150 K, the ϵ-Fe_2O_3 polymorph is a collinear ferrimagnet with magnetic moments directed along the *a* axis, whereas the magnetic ordering below 80 K is characterized by a square-wave incommensurate structure. The transformation between these two states is a second-order phase transition and involves subtle structural changes mostly affecting the coordination of the tetrahedral and one of the octahedral Fe sites. The temperature dependence of the ϵ-Fe_2O_3 magnetic properties is discussed in light of these results.

I. Introduction

Despite being known since 1934,[1] ϵ-Fe_2O_3 has been much less studied than other iron(III) oxides, such as the α and γ polymorphs. For instance, it was not until quite recently that an agreement was reached on describing its crystalline structure with an orthorhombic cell in the $Pna2_1$ space group.[2] The structure is isomorphous to $GaFeO_3$ and $AlFeO_3$ and presents four different Fe sites, three in octahedral and one in tetrahedral oxygen coordination. From the magnetic point of view, ϵ-Fe_2O_3 has long been known to be paramagnetic above 510 K and to present below this temperature an antiparallel arrangement of the Fe^{3+} cations,[2−5] characterized by a rather large anisotropy.[5] However, no in-depth studies have been carried out up to now to determine its magnetic structure. The interest in the magnetic properties of this material has been revived because the scenario disclosed by recent studies is unexpectedly rich and complex. Indeed, this oxide exhibits a huge room-temperature coercivity of about 20 kOe,[6,7] and a magnetic transition at low temperature.[8,9] This low-temperature transition leads to about 5% diminution in the saturation magnetization, M_s, and a reduction in the squareness ratio, M_r/M_s, from 0.5 to 0.2 on cooling from 150 to 85 K, where M_r is the remanent magnetization. Moreover, a large decrease in the coercivity, H_c, from 22.5 to 0.8 kOe is observed between 200 and 100 K[9] (see Figure 1). In

* To whom correspondence should be addressed. E-mail: mgich@icmab.es.

(1) Forrestier, H.; Guiot-Guillain, G. C. *C. R. Acad. Sci.* **1934**, *199*, 720.
(2) Tronc, E.; Chanéac, C.; Jolivet, J. P. *J. Solid State Chem.* **1998**, *139*, 93.
(3) Trautmann, J.-M.; Forestier, H. C. *C. R. Acad. Sci.* **1965**, *261*, 4423.
(4) Schrader, R.; Buttner, G. *Z. Anorg. Allg. Chem.* **1963**, *320*, 220.
(5) Dézsi, I.; Coey, J. M. D. *Phys. Status Solidi A* **1973**, *15*, 681.
(6) Jin, J.; Ohkoshi, S.; Hashimoto, K. *Adv. Mater.* **2004**, *16*, 48.
(7) Popovici, M.; Gich, M.; Nižňanský, D.; Roig, A.; Savii, C.; Casas, Ll.; Molins, E.; Zaveta, K.; Enache, C.; Sort, J.; de Brion, S.; Chouteau, G.; Nogués, J. *Chem. Mater.* **2004**, *16*, 5542.
(8) Kurmoo, M.; Rehspringer, J.-L.; Hutlova, A.; D'Órleans, C.; Vilminot, S.; Estournès, C.; Nižňanský, D. *Chem. Mater.* **2005**, *17*, 1106.
(9) Gich, M.; Frontera, C.; Roig, A.; Savii, C.; Casas, Ll.; Molins, E.; Zaveta, K.; Enache, C.; Sort, J.; de Brion, S.; Chouteau, G.; Nogués, J. *J. Appl. Phys.* **2005**, *98*, 044307.

10.1021/cm060993l CCC: $33.50
Published on Web 07/04/2006

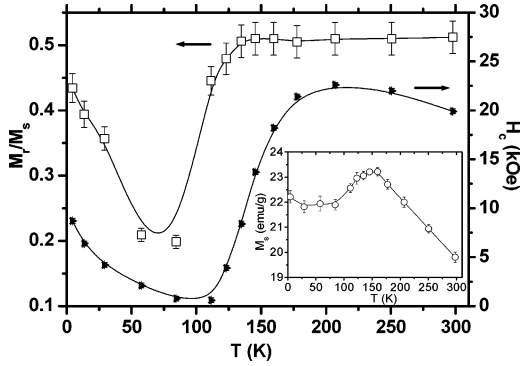

Figure 1. Temperature dependence of the coercive field H_C, the squareness ratio M_R/M_S, and the saturation magnetization M_S; (inset) in ϵ-Fe_2O_3 (taken from ref 9).

addition, the material presents a magnetoelectric coupling at about 100 K.[10]

Tronc et al. studied the ϵ-Fe_2O_3 magnetic structure at 9 K by means of in-field Mössbauer spectroscopy and proposed a nearly collinear ferrimagnetic order at the octahedral sites and a misalignment with possible disorder at the tetrahedral sites.[2] However, the presence of a magnetic transition, which is not observed in the $GaFeO_3$ and $AlFeO_3$ ferrimagnetic isomorphous systems,[11,12] was somehow overlooked in their work, and the large thermal dependence presented by the hyperfine field of the Fe tetrahedral site was ascribed to dynamical phenomena. The two groups that first reported on this low-temperature transition have interpreted it quite differently.[8,9] On the one hand, according to Kurmoo et al., all Fe^{3+} cations in ϵ-Fe_2O_3 carry the same magnetic moment and its room-temperature magnetic structure is that of a canted antiferromagnet that, on cooling to below 150 K, would undergo a Morin-like transition resulting in a second canted antiferromagnetic phase with smaller canting angles.[8] A similar interpretation to the transition has been given by Sakurai et. al, who also studied the ϵ-Fe_2O_3 structure by X-ray diffraction in a 60−293 K temperature range, although they were not able to reveal any structural change along the transition.[13] In contrast, we have proposed that at room-temperature, ϵ-Fe_2O_3 is a collinear ferrimagnet with the net magnetization arising from the lower magnetic moment of the Fe^{3+} in tetrahedral coordination; we have related the anomalies in the magnetic properties at low temperatures to the appearance of an incommensurate magnetic order, already indicated by preliminary neutron-diffraction experiments.[9] In the context described above, besides clarifying the nature of the ϵ-Fe_2O_3 magnetic structure below 100 K, we need to investigate a second question of whether the eventual occurrence of structural changes is associated with the transition. Indeed, understanding the relationship between the structural and magnetic properties of ϵ-Fe_2O_3 can be crucial to comprehending both the magnetic softening[9] and the coupling between magnetic and dielectric properties[10] that are observed in this oxide.

Thus, the aim of this work is to elucidate the high temperature (HT) and low temperature (LT) structures of ϵ-Fe_2O_3 and to shed some light into the nature of this transition. We present here a refinement of the crystal and magnetic structures of ϵ-Fe_2O_3 from X-ray and neutron powder-diffraction data that is complemented by Mössbauer spectroscopy, magnetization, and heat-capacity measurements.

II. Experimental Details

For the present study, we have used the ϵ-Fe_2O_3/amorphous SiO_2 nanocomposite sample that was already investigated in our previous work.[9] For the powder-diffraction measurements, new batches were prepared following the same procedure that has been described in detail elsewhere.[7] In some of these samples, small amounts (<10 wt %) of α-Fe_2O_3 were detected. To optimize the material structural characterization using diffraction, we removed the SiO_2 amorphous matrix by continuously stirring the sample in a concentrated NaOH solution (~12 M) at 80 °C. After 2 days, the solution was centrifuged; the sample was washed several times with distilled water until it achieved a neutral pH and was finally dried at 60 °C. X-ray diffraction analysis performed after this treatment revealed the complete removal of the SiO_2 amorphous matrix, whereas the ϵ-Fe_2O_3 phase remained unaltered. Neutron powder-diffraction (NPD) patterns were collected in the D20 instrument at the Institut Laue Langevin (Grenoble, France) using a 2.42 Å wavelength on heating at 1.7 K/min between 10 and 300 K. Synchrotron X-ray powder-diffraction (SXRPD) measurements were performed at fixed temperatures on heating in the same temperature range using the ID31 diffractometer of ESRF (Grenoble, France) with a 0.500 Å wavelength. The patterns were refined by the Rietveld method using the FullProf[14] program suite. The presence of small amounts of α-Fe_2O_3 was considered in the refinements, taking into account its different magnetic structure above and below the Morin transition (at about 240 K). However, this magnetic transition has not been further considered, because it takes place in a temperature well above the temperature range discussed herein. Mössbauer spectra were acquired at different temperatures between 10 and 300 K using a conventional transmission Mössbauer spectrometer with a ^{57}Co/Rh source. Velocity calibration was done using a 6 μm foil of metallic iron, and the Mössbauer parameters are given relative to this standard at room temperature. The program package NORMOS[15] was used to fit the spectra. Magnetization measurements were performed using a Quantum Design MPMS SQUID magnetometer. Measurements of the ac susceptibility (1 Oe, 33−1000 Hz) and heat capacity C_p, using a 2τ relaxation method, were carried out in a Quantum Design PPMS.

III. Results and Discussion

A. Neutron and X-ray Diffraction. In Figure 2, the NPD patterns of ϵ-Fe_2O_3 recorded at 200, 160, 80, and 10 K evidence a change in magnetic structure taking place between 160 and 80 K that is characterized by the disappearance of the (011), (110), (111), and (120) magnetic reflections and the development of satellites at either sides of these reflec-

(10) Gich, M.; Frontera, C.; Roig, A.; Fontcuberta, J.; Molins, E.; Bellido, N.; Simon, Ch.; Fleta, C. *Nanotechnology* **2006**, *17*, 687.
(11) Berthaut, E.; F.; Bassi, G.; Buisson, G.; Chappert, J.; Delapalme, A.; Pauthenet, R.; Rebouillat, H. P.; Aleonard, R. *J. Phys. (Paris)* **1966**, *7*, 28.
(12) Bouree, F.; Badour, J. L.; Elabraoui, E.; Musso, J.; Laurent, C.; Rousset, A. *Acta Crystallogr., Sect. B* **1996**, *52*, 217.
(13) Sakurai, S.; Jin, J.; Hashimoto, K.; Ohkoshi, S. *J. Phys. Soc. Jpn.* **2005**, *74*, 1946.
(14) Rodriguez-Carvajal, J. *Physica B* **1993**, *192*, 55.
(15) Brand, R. A. *Nucl. Instrum. Methods Phys. Res., Sect. B* **1987**, *28*, 398.

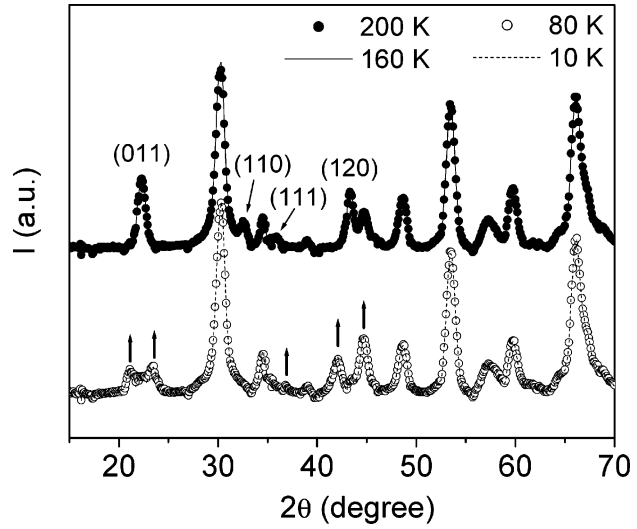

Figure 2. NPD patterns corresponding to the HT (200 and 160 K) and LT (80 and 10 K) phases of ϵ-Fe_2O_3. The up arrows indicate the satellites emerging in the LT phase.

tions. The changes observed in the NPD patterns of Figure 2 affect only some of the magnetic reflections, suggesting that the transformation does not involve major structural changes. Whereas the HT phase of ϵ-Fe_2O_3 (200 and 160 K patterns) can be refined using the magnetic and nuclear structures of $AlFeO_3$ as a starting model,[12] the new peaks that characterize the magnetic structure of the LT phase can be indexed with an incommensurate propagation vector $\mathbf{k} = (0, 0.1047, 0)$.

The small crystallite size of the ϵ-Fe_2O_3 nanoparticles (less than 20 nm) causes a peak broadening and therefore a strong peak overlap, which reduces the number of effective reflections. A multipattern approach using both NPD and SXRPD patterns recorded at 200 and 10 K was used to attempt a reliable refinement of nuclear and magnetic structures of the HT and LT phases of ϵ-Fe_2O_3, respectively. Besides ϵ-Fe_2O_3, the nuclear and magnetic structures of α-Fe_2O_3, representing less than 10 wt % of the sample, were also considered in the refinements. The comparisons between the experimental and calculated data obtained with the joint Rietveld refinement of the SXRPD and NPD patterns at 200 and 10 K are presented in Figures 3 and 4, respectively. The refined atomic coordinates for the 10 nonequivalent atomic sites at 200 and 10 K, together with the standard reliability factors, are given in Table 1. As is found for isostructural phases $GaFeO_3$, $AlFeO_3$, and κ-Al_2O_3, which have been previously refined,[16,12,17] the cation coordination polyhedra are two distorted[18] and one regular octahedra and one tetrahedron. Therefore, the different Fe^{3+} sites are hereafter referred as Fe_{DO1}, Fe_{DO2}, Fe_{RO}, and Fe_T (where DO stands for distorted octahedral, RO for regular octahedral and T for tetrahedral

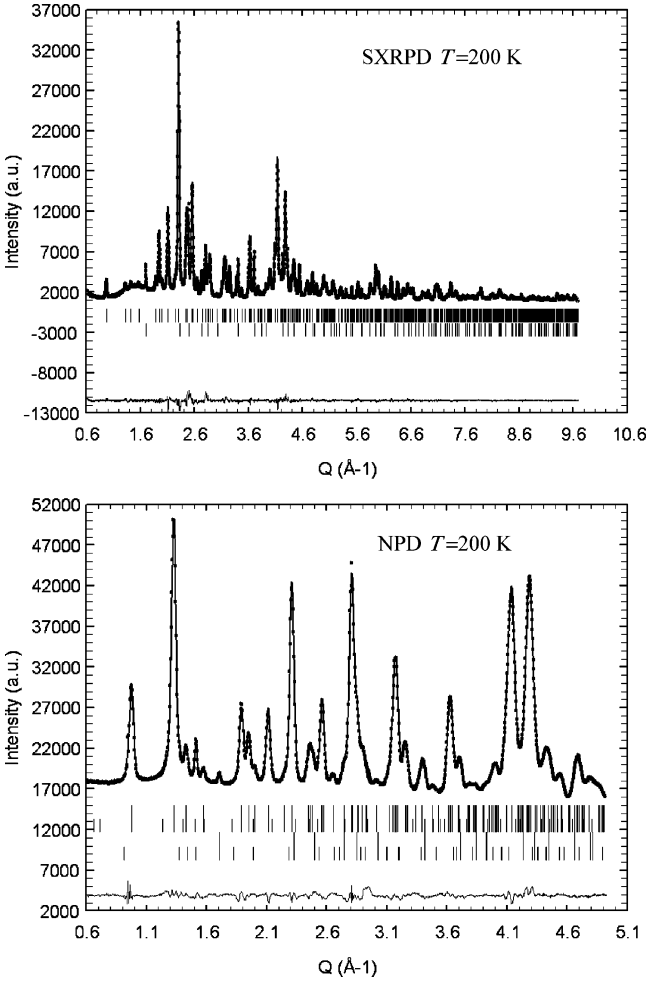

Figure 3. Experimental (■), calculated (solid line), and difference (lower line) plots for the joint refinement of SXRPD and NPD patterns of ϵ-Fe_2O_3 collected at 200 K (upper and lower panels, respectively). Reflection positions of the different phases are indicated by vertical bars in the following descending order: ϵ-Fe_2O_3, α-Fe_2O_3 for the upper panel and ϵ-Fe_2O_3, ϵ-Fe_2O_3 magnetic, α-Fe_2O_3 and α-Fe_2O_3 magnetic for the lower panel.

coordinations). In Figure 5, the coordination octahedra of Fe_{DO1} and Fe_{DO2} are represented in black and dark gray, respectively, whereas the Fe_{RO} and Fe_T environments are represented in light gray. As expected, the changes between the asymmetric units of the HT and LT phases are in general small, although the *z* coordinate of O2 significantly increases on cooling from 200 to 10 K (see Table 1). As can be seen from Figure 5 (black spheres), the 0.3 Å displacement of O2 along *c* is responsible for the increased tilting of the Fe_{DO1} and Fe_T coordination polyhedra in the LT structure. The bonding distances and angles calculated from cell parameters and asymmetric units reported in Table 1 (see Tables 2 and 3) reveal other features that can be relevant to understanding the HT → LT magnetic transition. On one hand, it is found that on cooling from 200 to 10 K, there is an increase in the bonding distances of both Fe_T with O4, O6 and Fe_{DO2}, Fe_{RO} with O2, the latter showing an average expansion of about 1%. In the case of the tetrahedral site, the elongation of the apical Fe_T−O4 distance shows a 2.2% variation. On the other hand, the distortions of the Fe_T and Fe_{DO1} polyhedra, which are more affected by the HT → LT transition, increase from 2.4×10^{-4} to 6.8×10^{-4} and from 71.3×10^{-4} to $84.3 \times$

(16) Abrahams, S. C.; Reddy, J. M. Bernstein, J. L. *J. Chem. Phys.* **1965**, *42*, 3957.
(17) Smrèok, L.; Langer, V.; Halvarsson, M.; Ruppi, S. *Z. Kristallogr.* **2001**, *216*, 409.
(18) The distortion of a coordination polyhedron of a cation is defined as $1/n\sum_{i=1}^{n}[(d_i - \langle d\rangle)/\langle d\rangle]^2$, where d_i is the distance to a given neighbor, $\langle d\rangle$ the average distance to the first neighbor, and *n* is the coordination number. At 200 K, the distortions of Fe_{DO-1}, Fe_{DO-2}, Fe_{RO}, and Fe_T have been found to be 71.3×10^{-4}, 58.4×10^{-4}, 2.4×10^{-4}, and 4.6×10^{-4}, respectively.

Table 1. Cell Parameters and Asymmetric Units of ϵ-Fe_2O_3 at 200 and 10 K, Together with the Reliability Parameters of the Multipattern Rietveld Refinement Expressed in Percent (except for χ^2)

$T = 200$ K[a]				$T = 10$ K[b]			
atom	*x*/*a*	*y*/*b*	*z*/*c*	atom	*x*/*a*	*y*/*b*	*z*/*c*
O1	0.978(2)	0.3282(15)	0.4314(11)	O1	0.978(4)	0.331(3)	0.4288(17)
O2	0.515(2)	0.4907(17)	0.4187(16)	O2	0.512(3)	0.4871(20)	0.4489(14)
O3	0.650(3)	0.9979(13)	0.1883(9)	O3	0.646(4)	0.9943(20)	0.1871(14)
O4	0.160(3)	0.1637(15)	0.1956(7)	O4	0.159(4)	0.162(2)	0.2002(11)
O5	0.841(3)	0.1680(15)	0.6669(7)	O5	0.858(3)	0.157(3)	0.6685(12)
O6	0.527(2)	0.1637(19)	0.9362(9)	O6	0.523(4)	0.161(3)	0.9257(15)
Fe_{DO1}	0.1928(11)	0.1506(6)	0.5807(3)	Fe_{DO1}	0.1931(17)	0.1514(10)	0.5820(4)
Fe_{DO2}	0.6826(6)	0.0291(3)	0.7897(5)	Fe_{DO2}	0.6867(10)	0.0283(4)	0.7938(8)
Fe_T	0.1858(10)	0.1519(6)	0.0000	Fe_T	0.1852(15)	0.1526(9)	0.0000
Fe_{RO}	0.8104(7)	0.1580(4)	0.3071(3)	Fe_{RO}	0.8098(10)	0.1592(6)	0.3079(5)

[a] Parameters: $a = 5.0885(5)$ Å, $b = 8.7802(14)$ Å, $c = 9.4709(13)$ Å. Reliability parameters (in % except for χ^2): SXRPD $R_B = 2.26$, $R_{wp} = 3.59$, $R_{exp} = 1.94$, $\chi^2 = 3.43$; NPD $R_B = 1.41$, $R_{Mag} = 1.89$, $R_{wp} = 4.00$, $R_{exp} = 1.33$. [b] Parameters: $a = 5.085(1)$, $b = 8.774(2)$, $c = 9.468(2)$. Reliability parameters (in % except for χ^2): SXRPD $R_B = 2.98$, $R_{wp} = 7.33$, $R_{exp} = 3.66$, $\chi^2 = 4.015$. NPD $R_B = 3.85$, $R_{Mag} = 6.33$, $R_{wp} = 7.60$, $R_{exp} = 1.40$.

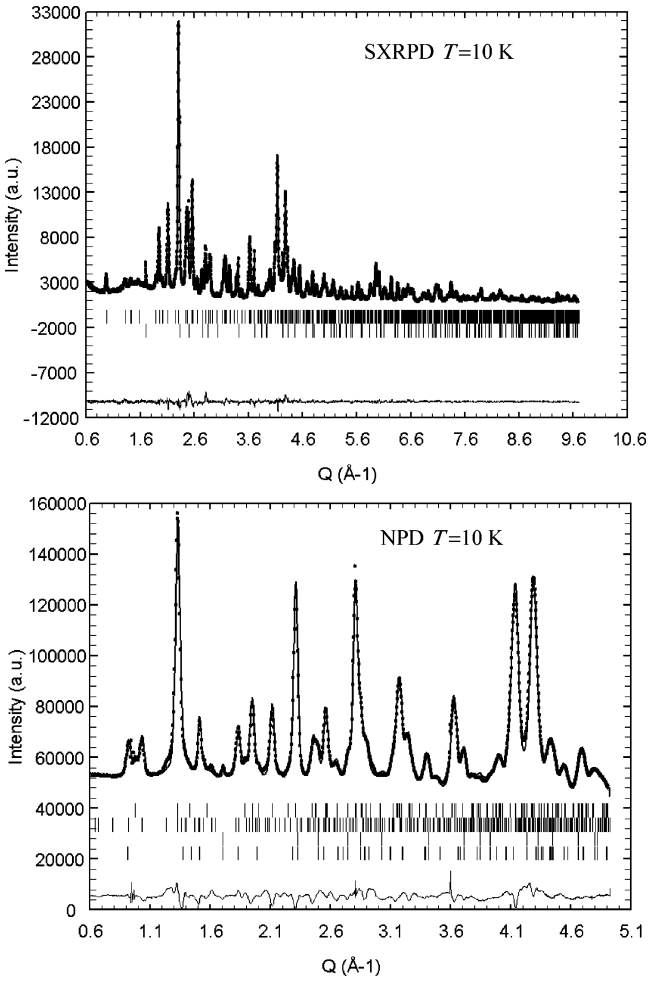

Figure 4. Experimental (■), calculated (solid line), and difference (lower line) plots for the joint refinement of SXRPD and NPD patterns of ϵ-Fe_2O_3 collected at 10 K (upper and lower panels, respectively). Reflection positions of the different phases are indicated by vertical bars in the following descending order: ϵ-Fe_2O_3 and α-Fe_2O_3 for the upper panel and ϵ-Fe_2O_3, ϵ-Fe_2O_3 magnetic, α-Fe_2O, and α-Fe_2O_3 magnetic for the lower panel.

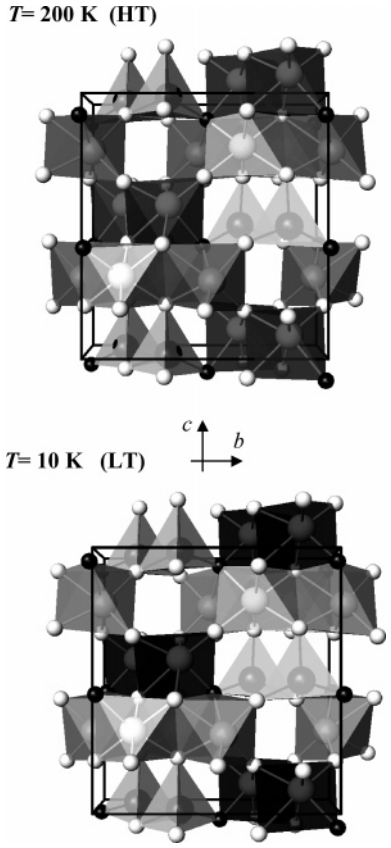

Figure 5. Perspective view of the ϵ-Fe_2O_3 HT and LT structures along the [100] direction (upper and lower panels, respectively).The coordination octahedra of Fe_{DO1}, Fe_{DO2}, and Fe_{RO} are black, gray, and light gray, respectively, and the oxygen atoms are represented by small spheres. The main structural changes concern the orientations of the coordination polyhedra of Fe_{DO1} (black octahedron) and Fe_T (light gray tetrahedron) due to the displacement of O2 (in black) along *c*.

10^{-4}, respectively, with the Fe_{DO1}−O2 distance decreasing by about 10%.

Regarding the magnetic structures, the model that yielded the best fits for the HT phase is one in which the magnetic moments *m* are along the *a* axis with $m_{HT}(Fe_{DO1}) = -3.9\mu_B$, $m_{HT}(Fe_{DO2}) = 3.9\mu_B$, $m_{HT}(Fe_T) = -2.4\mu_B$, and $m_{HT}(Fe_{RO}) = 3.7\mu_B$. The refinement was performed using the constraint $m_{HT}(Fe_{DO1}) = -m_{HT}(Fe_{DO2})$ suggested by Mössbauer spectroscopy measurements (see section B below). Thus, the ϵ-Fe_2O_3 HT magnetic structure presents the *m′m2′* point group and is represented in Figure 6. The antiferromagnetic coupling between the different magnetic moments yields a net magnetization of $0.3\mu_B$ per Fe^{3+}, in agreement with the M_s values of ϵ-Fe_2O_3 at 200 K.[9] It is interesting to note that the NPD data can be also simulated allowing small *y* and *z* components for the Fe_T and Fe_{RO} moments (i.e., a small canting), although this did not result in any improvement in the fit. However, the fact that the NPD data do not exclude small canting of the Fe_T and Fe_{RO} spins would be in agreement with the thermal fluctuations in these sites,

Table 2. Coupling Angles between the Different Fe Sites and Fe−O Distances (given in Å) at 200 K and 10 K (italics)

O1

	Fe_{DO1}	$Fe_{DO1}b$	$Fe_{DO2}a$	Fe_{RO}	$Fe_{RO}b$
Fe_{DO1}	2.372(13), *2.41(2)*				
$Fe_{DO1}b$	88.5(5), *86.8(9)*	2.035(11), *2.056(20)*			
$Fe_{DO2}a$	171.5(5), *171.9(9)*	94.6(5), *94.5(9)*	2.362(13), *2.31(2)*		
Fe_{RO}	93.1(5), *92.5(9)*	99.6(5), *98.8(9)*	94.2(5) *95.1(9)*	2.085(12), *2.08(2)*	
$Fe_{RO}b$	90.1(5), *89.4(8)*	167.2(5), *167.2(9)*	85.2(5), *87.6(8)*	93.2(5), 93.5(9)	2.064(11), *2.041(20)*

O2

	$Fe_{DO1}b$	$Fe_{DO2}a$	Fe_Ta	$Fe_{RO}b$
$Fe_{DO1}b$	2.171(15), *1.976(17)*			
$Fe_{DO2}a$	102.0(6), *102.1(8)*	1.994(13), *2.149(16)*		
Fe_Ta	111.2(7), *125.0(10)*	122.4(6), *116.0(8)*	1.908(15), *1.833(18)*	
$Fe_{RO}b$	102.7(6), *104.8(7)*	101.0(6), *91.0(7)*	115.1(7), *112.2(8)*	1.976(14), *2.121(16)*

O3

	$Fe_{DO1}c$	$Fe_{DO2}c$	Fe_{RO}
$Fe_{DO1}c$	1.838(12), *1.817(19)*		
$Fe_{DO2}c$	124.2(7), *126.6(10)*	1.960(14), *1.976(20)*	
Fe_{RO}	129.8(6), *128.6(9)*	*99.4(6), 97.8(8)*	1.977(12), *2.026(18)*

O4

	$Fe_{DO2}c$	Fe_T	Fe_{RO}	$Fe_{RO}b$
$Fe_{DO2}c$	2.074(13), *2.047(18)*			
Fe_T	110.8(5), *111.7(7)*	1.860(7), *1.902(11)*		
Fe_{RO}	95.3(6), *96.1(8)*	124.6(5), *123.8(7)*	2.069(14), *2.048(19)*	
$Fe_{RO}b$	105.0(5), *105.6(7)*	122.2(5), *120.6(7)*	94.4(6), *95.0(8)*	2.038(13), *2.022(17)*

O5

	Fe_{DO1}	$Fe_{DO1}b$	Fe_{DO2}
Fe_{DO1}	1.973(15), *1.891(17)*		
$Fe_{DO1}b$	104.0(7), *102.5(10)*	1.942(14), *2.05(2)*	
Fe_{DO2}	126.8(7), *133.2(10)*	129.0(6), *124.2(10)*	1.868(12), *1.855(20)*

O6

	Fe_{DO2}	Fe_T	Fe_Tb
Fe_{DO2}	1.987(13), *1.90(2)*		
Fe_T	124.8(6), *129.0(10)*	1.841(11), *1.86(2)*	
Fe_Tb	123.9(7), *124.2(11)*	110.1(7), *106.6(11)*	1.908(16), *1.96(3)*

[a] Transformations: a = ($^1/_2 - x$, $y - ^1/_2$, $z - ^1/_2$); b = ($^1/_2 - x$, $^1/_2 - y$, z); c = ($-x$, $-y$, $z + ^1/_2$).

recently reported by Tronc et al.[19] For the LT phase, different helimagnetic and sine-modulated structures have been tested to account for the magnetic structure associated with **k**. The best fit has been obtained for a sine-modulated structure with a periodicity of about 10 crystalline unit cells and with all the magnetic moments lying in the *xy* plane. As in the HT structure, $m_{LT}(Fe_{DO1})$ and $m_{LT}(Fe_{DO2})$ were constrained to be antiparallel and directed along the *x* direction, whereas $m_{LT}(Fe_T)$ and $m_{LT}(Fe_{RO})$ are mainly oriented in opposite directions along *x* and present small *y* components. However, for the LT structure, the symmetry analysis imposes that all the magnetic atoms are split into two orbits, and the fact that the structure is sine-modulated introduces magnetic phases. This results in an increased number of refinable magnetic parameters that increase the difficulty of finding an appropriate model for the magnetic structure from the small number of measurable magnetic reflections. All the magnetic moments obtained in our best fit of the NPD pattern at LT using a simple sine-wave-modulated structure increase with respect to those of the HT structure. The values of some of them are, however, clearly nonphysical, exceeding the $5\mu_B$ expected for an Fe^{3+} cation.

B. Mössbauer Spectroscopy. Mössbauer spectroscopy gives additional information that can be complementary to the NPD data. In Figure 7, it can be observed that the Mössbauer spectra of ϵ-Fe_2O_3 change on cooling through the HT → LT transition, especially because of the evolution of the Fe_T subspectrum (dotted line). According to the crystalline structure of ϵ-Fe_2O_3, the spectra were fitted assuming that each of the four Fe sites contributed to the spectra with a sextet. In particular, the spectra could be fitted by constraining the hyperfine fields, B_{hf}, and the widths of the Fe_{DO1} and Fe_{DO2} contributions to be equal, in accordance with the NPD results. Figure 8a shows the temperature dependence of the hyperfine parameters for the different Fe sites in the 10−200 K range. Between 150 and 80 K, most of the hyperfine parameters of the different Fe sites deviate from the thermal dependence displayed at higher temperatures. These anomalies are particularly important for Fe_T, which displays a 20% increase in B_{hf} between 140 and 100 K and a shift in both the isomer shift, δ, and the quadrupole splitting, Δ, in the same temperature range. Below 150 K,

(19) Tronc, E.; Chanéac, C.; Jolivet, J. P.; Grenèche, J. M. *J. Appl. Phys.* **2005**, *98*, 053901.

Table 3. Bonding Angles in the Coordination Polyhedra for the four Fe Sites of ϵ-Fe_2O_3 at 200 and 10 K[a]

	200 K	10 K		200 K	10 K
O2a−Fe_T−O4	113.9(10)	105.0(12)	O1−Fe_{DO1}−O1b	81.6(7)	81.1(13)
O2a−Fe_T−O6	114.5(10)	116.1(17)	O1−Fe_{DO1}−O2b	76.2(8)	78.9(13)
O2a−Fe_T−O6b	106.0(13)	109.5(18)	O1−Fe_{DO1}−O3c	175.9(10)	175.8(17)
O4−Fe_T−O6	113.0(8)	116.1(13)	O1−Fe_{DO1}−O5	77.2(7)	80.5(12)
O4−Fe_T−O6b	103.8(9)	107.0(13)	O1−Fe_{DO1}−O5b	83.7(7)	83.7(12)
O6−Fe_T−O6b	104.3(10)	102.7(18)	O1b−Fe_{DO1}−O2b	81.9(8)	85.6(13)
			O1b−Fe_{DO1}−O3c	98.0(8)	96.9(13)
O1−Fe_{RO}−O1b	88.3(7)	90.0(15)	O1b−Fe_{DO1}−O5	158.0(11)	159.8(15)
O1−Fe_{RO}−O2b	87.5(9)	83.8(14)	O1b−Fe_{DO1}−O5b	86.6(8)	86.1(13)
O1−Fe_{RO}−O3	179.5(10)	179.0(18)	O2b−Fe_{DO1}−O3c	99.7(10)	97.3(12)
O1−Fe_{RO}−O4	85.4(8)	84.8(12)	O2b−Fe_{DO1}−O5	87.6(9)	82.8(11)
O1−Fe_{RO}−O4b	84.0(7)	82.6(12)	O2b−Fe_{DO1}−O5b	158.1(12)	161.6(17)
O1d−Fe_{RO}−O2b	99.5(9)	94.3(13)	O3c−Fe_{DO1}−O5	102.7(11)	100.9(15)
O1d−Fe_{RO}−O3	91.6(8)	90.3(12)	O3c−Fe_{DO1}−O5b	100.4(10)	100.0(17)
O1d−Fe_{RO}−O4	173.7(11)	174.7(17)	O5−Fe_{DO1}−O5b	96.6(11)	100.0(15)
O1d−Fe_{RO}−O4b	86.7(7)	86.4(12)			
O2c−Fe_{RO}−O3	93.0(9)	97.2(11)	O1a−Fe_{DO2}−O2a	78.0(7)	75.7(11)
O2c−Fe_{RO}−O4	80.6(9)	84.2(10)	O1a−Fe_{DO2}−O3c	83.6(7)	84.2(12)
O2c−Fe_{RO}−O4b	169.3(12)	166.4(14)	O1a−Fe_{DO2}−O4c	76.6(7)	76.5(11)
O3−Fe_{RO}−O4	94.7(10)	94.9(14)	O1a−Fe_{DO2}−O5	172.1(10)	168.7(19)
O3−Fe_{RO}-O4b	95.5(9)	96.5(13)	O1a−Fe_{DO2}−O6	84.8(9)	86.4(17)
O4−Fe_{RO}−O4b	92.3(10)	93.9(14)	O2a−Fe_{DO2}−O3c	161.1(12)	159.9(15)
			O2a−Fe_{DO2}−O4c	80.1(8)	83.5(10)
			O2a−Fe_{DO2}−O5	99.1(10)	101.9(12)
			O2a−Fe_{DO2}−O6	88.9(9)	88.0(13)
			O3c−Fe_{DO2}−O4c	91.4(10)	91.4(14)
			O3c−Fe_{DO2}−O5	98.4(11)	97.8(15)
			O3c−Fe_{DO2}−O6	94.0(9)	91.3(13)
			O4c−Fe_{DO2}−O5	95.7(10)	92.3(16)
			O4c−Fe_{DO2}−O6	159.9(11)	162.3(18)
			O5−Fe_{DO2}−O6	102.6(8)	104.7(13)

[a] Transformations: a = ($^1/_2 - x$, $y - {}^1/_2$, $z - {}^1/_2$); b = ($^1/_2 - x$, $^1/_2 - y$, z); c = ($-x$, $-y$, $z + {}^1/_2$).

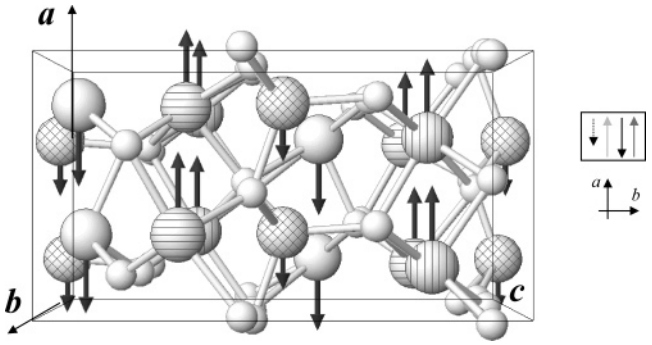

Figure 6. Magnetic structure of the ϵ-Fe_2O_3 HT phase, where the Fe_{DO1}, Fe_{DO2}, Fe_{RO}, and Fe_T atoms are distinguished by plain, horizontal stripes, vertical stripes, and cross-hatch patterns, respectively. The magnetic moments of the Fe_{DO1}, Fe_{DO2}, Fe_{RO}, and Fe_T sites are schematically represented in the figure by black, gray, light gray, and dotted arrows, respectively.

B_{hf} decreases by ~4% for Fe_{RO} between 150 and 110 K and by ~3.5% for Fe_{DO1} and Fe_{DO2} between 150 and 130 K. Note that for Fe_{DO1}, Δ changes from negative to positive values in this interval of temperatures and that below 130 K, δ decreases with temperature for this particular site, in contrast with the usual temperature dependence of the isomer shift. The latter results suggest that on cooling below 150 K, some structural changes would affect the Fe_{DO1} coordination octahedron, which, subsequently, would induce changes in the coordination of the Fe_T site. Indeed, this interpretation is compatible with the results obtained from the diffraction experiments, which revealed that the HT → LT transition results in an increased tilting and distortion of the Fe_{DO1} and Fe_T coordination polyhedron. It is worth pointing out that large changes in Δ can be also due to spin reorientations. Although the NPD results seem to indicate that the HT → LT transition has little effect in the direction of the Fe_{DO1} magnetic moment, the LT magnetic structure would be needed to ascribe the sign change in Δ for this site exclusively to structural changes.

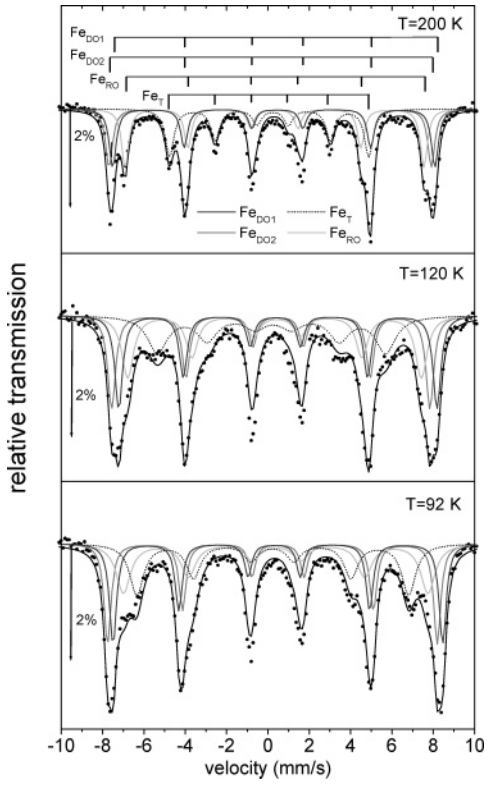

Figure 7. Mössbauer spectra of ϵ-Fe_2O_3 at 200, 120, and 92 K. The subspectra correspond to the different Fe sites in the ϵ-Fe_2O_3 structure and are schematically presented at the top of the figure.

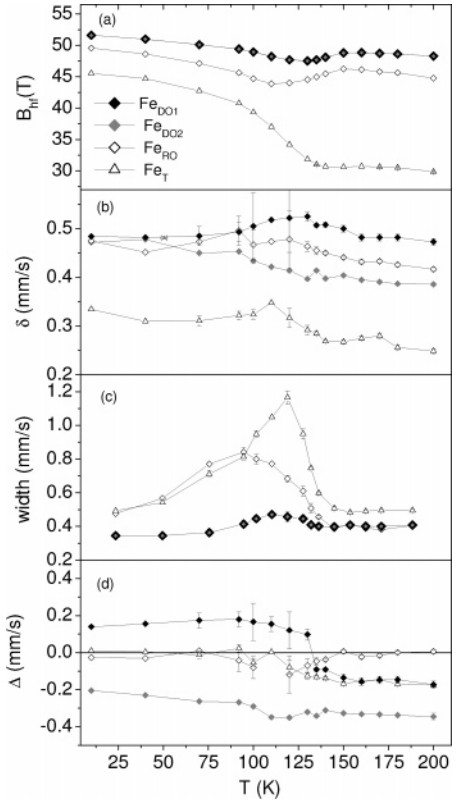

Figure 8. Temperature dependence of the (a) hyperfine field (B_{hf}), (b) isomer shift (δ), (c) sextet line width (width), and (d) quadrupolar splitting (Δ) of the different Fe sites of ϵ-Fe_2O_3 obtained from Mössbauer spectra.

The structural transformations occurring below 150 K might be responsible for the magnetic softening of the system that is reported in Figure 1. Interestingly, the changes observed in Δ for both the Fe_{DO1} and Fe_T sites can be related to modifications in the spin−orbit coupling of the Fe cations, which are responsible for the magnetic anisotropy of a magnetic system. In contrast, in the case of the Fe_T site, the substantial elongation of the apical Fe_T−O4 occurring along the HT → LT transformation could be responsible for the large increase in B_{hf} observed at this site, which in turn indicates an increment of the Fe_T magnetic moment,[20] also deduced from the analysis of the NPD data at 10 K. This can explain the M_s diminution observed below 150 K (see Figure 1 inset), because the Fe_T and Fe_{RO} are antiferromagnetically coupled and the increase in B_{hf} at the Fe_T site is larger than the B_{hf} increase experienced by Fe_{RO}. Regarding the hyperfine fields, it is also interesting to note that the ratio between the B_{hf} values for different Fe sites at 200 K (i.e., $B_{hf}(Fe_{DO1})/B_{hf}(Fe_T) = 1.63$, $B_{hf}(Fe_{RO})/B_{hf}(Fe_T) = 1.56$) is in good agreement with the corresponding ratio of magnetic moments obtained from the analysis of the NPD data. Assuming that the proportionality between B_{hf} and m still holds for the LT phase and combining the m_{HT} values obtained from the NPD pattern at 200 K with the B_{hf} at 10 K, we can estimate the magnetic moments for the LT phase to be $m_{LT}(Fe_{DO1}) = -4.2\mu_B$, $m_{LT}(Fe_{DO2}) = 4.2\mu_B$, $m_{LT}(Fe_T) = -3.7\mu_B$, and $m_{LT}(Fe_{RO}) = 4.1\mu_B$, in clear disagreement with the unrealistic values obtained from our best-fit model.

(20) Preston, R. S.; Hanna, S. S.; Heberle, J. *Phys. Rev.* **1962**, *128*, 2207.

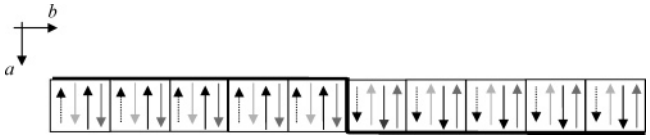

Figure 9. Simplified schematic representation of the square-wave magnetic structure of the LT phase of ϵ-Fe_2O_3. The magnetic moments of the Fe_{DO1}, Fe_{DO2}, Fe_{RO}, and Fe_T sites are schematically represented by black, gray, light gray, and dotted arrows, respectively.

In this regard, the temperature dependence of the Mössbauer subspectra line width (see Figure 8c) can shed some light on the deficiencies of our preliminary model for the LT magnetic structure of ϵ-Fe_2O_3. On cooling below 150 K, a sextet line width broadening is observed for all Fe sites but specially for Fe_T, which is due to the appearance of some disorder at the different crystallographic sites and indicates that the transformation is rather broad and that several phases can coexist in the 150−92 K interval. However, as T is further decreased, the line width values decrease progressively. Interestingly, at about 10 K, the line width values for all the sites are only slightly larger than those at 200 K, implying that the Mössbauer components for all the sites are quite narrow and, consequently, that the corresponding magnetic moments throughout the structure should be almost constant in modulus. However, this is not what one would expect if the LT magnetic structure of ϵ-Fe_2O_3 is supposed to be sine-modulated with a periodicity of about 10 unit cells. In this case, because for the $Pna2_1$ space group there is only one Wyckoff position of 4-fold multiplicity, an average of 40 atoms for every Fe site with magnetic moments ranging from zero to a maximum value are involved in one period of the amplitude-modulated structure, which would yield a broad hyperfine field distribution. Because the helical or spiral structures with constant m modulus that could account for the narrow Mössbauer lines of the LT phase are not consistent with the NPD data, the only magnetic structure that can make both the Mössbauer and the diffraction data compatible is a square-wave-modulated structure, i.e., the superposition of a series of sine-modulated structures having the harmonics of **k** as propagation vectors. In fact, the exceedingly large magnetic moments obtained when a single sine wave was considered might be reduced by taking into account the amplitudes of the different Fourier components. Thus, to determine the exact magnetic structure, it would be necessary to identify the higher-order reflections and determine the new propagation vectors, but this cannot be carried out because of the peak overlapping and the low intensity of the harmonic reflections. However, on the grounds of the above discussion, one may consider the structure represented in Figure 9 to be a simplified schematic model of the LT magnetic cell.

C. Magnetization and Heat-Capacity Measurements. The results presented in section B indicate that the HT → LT transformation in ϵ-Fe_2O_3 takes place in a broad temperature range and suggest that it consists of a succession of magnetic and structural changes. In this section, we present magnetic and heat-capacity measurements that give some details about the nature of the transition. Figure 10a shows the temperature dependence of the ϵ-Fe_2O_3 zero-field-cooling (ZFC) magnetization under 100 and 1000 Oe applied fields,

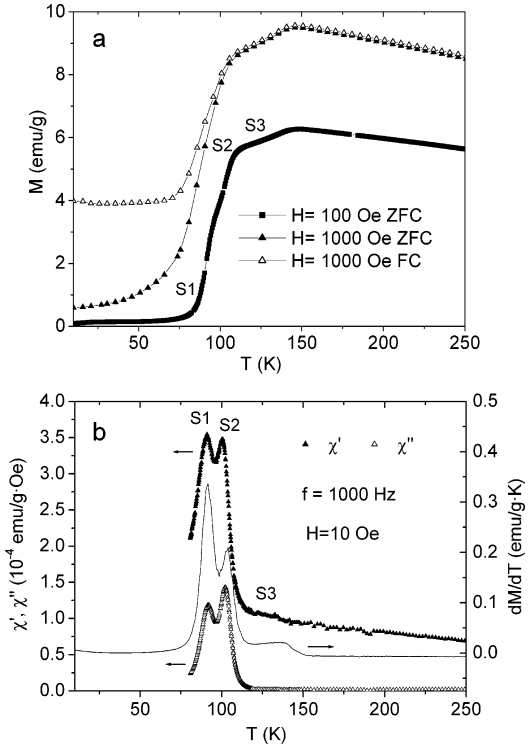

Figure 10. (a) Zero-field cooling (ZFC) and field cooling (FC) measurements of the temperature dependence of the magnetization in 100 and 1000 Oe applied fields. (b) Temperature dependence of the in-phase (▲) and out-of-phase (△) components of ϵ-Fe_2O_3 ac-susceptibility measured at 1000 Hz and 10 Oe field amplitude. The solid line is the temperature derivative of the $M_{100}^{ZFC}(T)$ curve presented in panel (a).

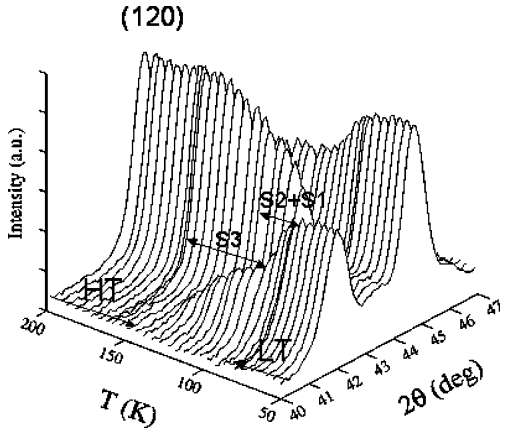

Figure 11. Temperature dependence of the (120) magnetic reflection and its satellites of ϵ-Fe_2O_3.

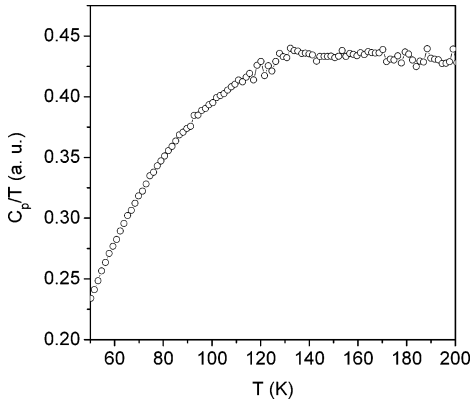

Figure 12. Temperature dependence of the ϵ-Fe_2O_3 heat capacity vs temperature.

$M_{100}^{ZFC}(T)$ and $M_{1000}^{ZFC}(T)$, respectively, together with the field-cooling (FC) measurement in 1000 Oe, $M_{1000}^{FC}(T)$. Upon heating from 10 K, $M_{100}^{ZFC}(T)$ presents an important increase between 85 and 150 K that takes place in three stages, if one considers the changes of the $M_{100}^{ZFC}(T)$ slope, in three temperature ranges ΔT_1 (85 K < T < 95 K), ΔT_2 (95 K < T < 110 K) and ΔT_3 (110 K < T < 147 K), the slope being much steeper in ΔT_1 and ΔT_2 than in ΔT_3. When the ZFC magnetization is measured in a field 10 times larger (see the $M_{1000}^{ZFC}(T)$ curve), the larger magnetization step starts at a lower temperature and is more gradual; it is also no longer possible to clearly distinguish between the first two stages. In contrast, no shift is observed for the magnetization stage in ΔT_3, which now presents a somewhat larger slope. Moreover, the FC measurement (see $M_{1000}^{FC}(T)$ curve) shows that the magnetic behavior below 110 K is irreversible even for small fields such as 1000 Oe, in contrast to the reversibility observed above this temperature. These measurements suggest that on heating, the transition from the LT to the HT magnetic structure of ϵ-Fe_2O_3 takes place in three consecutive stages occurring in ΔT_1, ΔT_2, and ΔT_3, hereafter referred as S1, S2, and S3, respectively. The measurements of Figure 10a evidence a distinct magnetic character of S1 and S2 as compared to S3, which is also confirmed by the temperature dependence of the magnetic AC susceptibility, χ. Namely, in Figure 10b, the temperature dependence of both the in-phase, $\chi'(T)$, and out of phase, $\chi''(T)$, components of ac susceptibility present sharp peaks at about 91 and 101 K, signaling the S1 and S2 transformations, respectively. Indeed, the susceptibility peaks coincide with the maxima in the temperature derivative of $M_{100}^{ZFC}(T)$ (solid line in Figure 10b), i.e., with the maximum slopes of $M_{100}^{ZFC}(T)$ in ΔT_1 and ΔT_2. On the other hand, for ΔT_3, only a barely observable shoulder occurs in $\chi'(T)$, whereas $\chi''(T)$ is zero. The magnetic measurements presented in Figure 10 are in agreement with the occurrence of magnetic and structural changes along ΔT_3 that can be inferred from the anomalies in the Mössbauer hyperfine parameters in this temperature interval. Thus, S3 is to be associated to the latter transformation, which in turn induces S2 and S1 at lower temperatures, which are predominantly related to a magnetic transition displaying a field-dependent behavior. The distinct magnetic nature of S3 on the one hand and S2 + S1 on the other is also revealed in Figure 11 by the temperature dependence of the NPD patterns. On cooling below 200 K, the intensity of the (120) magnetic reflection slightly decreases, with this diminution becoming much more pronounced below 150 K, coinciding with the gradual appearance of the satellites that characterize an incommensurate order (S3). Below 110 K, the intensity of the satellites suddenly increases (S2 + S1), resulting in the LT magnetic structure of ϵ-Fe_2O_3, which is fully developed at about 80 K. Heat-capacity measurements provide an additional evidence of the different characteristics of S3 with respect to S2 and S1. The temperature dependence of C_p/T represented in Figure 12 shows an anomaly around 130 K (i.e., in S3) and two distinct regimes above and below this temperature. Because $C_p/T = -\partial^2 G/\partial T^2$, where G is the free

energy, the anomaly in C_p/T suggests that S3 is related with a second-order magnetic and structural transition, which is supported by the absence of thermal hysteresis both in the magnetic (Figure 10) and dielectric[10] measurements.

IV. Conclusion

In conclusion, the HT magnetic structure of ϵ-Fe_2O_3 is that of a collinear ferrimagnetic material with the Fe^{3+} magnetic moment antiferromagnetically coupled along *a*. The Fe^{3+} magnetic moments in the Fe_{DO1} and Fe_{DO2} distorted octahedral positions mutually cancel, and the net magnetization of this phase results from the uncompensated magnetic moment of the atoms in tetrahedral (Fe_T) and regular octahedral (Fe_{RO}) positions. Between 150 and 80 K, ϵ-Fe_2O_3 undergoes magnetic and structural phase transformations that bring about a gradual decrease in the magnetic anisotropy. This transition takes place in at least three stages. Between 150 and 110 K, there are evidences of a second-order structural transition presumably involving the changes in the coordination of the Fe_{DO1} and Fe_T sites, occurring simultaneously with the emergence of an incommensurate magnetic order. The magnetic structure undergoes several transformations as the temperature is further decreased, but no additional changes are observed below 80 K. The combination of powder-diffraction and Mössbauer spectroscopy measurements indicate that ϵFe_2O_3 presents a square-wave incommensurate magnetic structure at LT.

Acknowledgment. Financial support from Ministerio de Educación y Ciencia, Projects MAT2003-01052 and MAT2004-01679, and Generalitat de Catalunya, Projects 2005SGR00452 and 2005SGR00401, is gratefully acknowledged. C.F. acknowledges financial support from MEC (Spain). W.A.A.M. acknowledges support from CNPq (Brazil). We acknowledge the ESRF and the ILL for the provision of X-ray and neutron beam time. We also thank F. Fauth for his assistance during XRD data collection.

CM060993L